Journal of Materials Chemistry A

RSC Publishing

PAPER

View Article Online
View Journal | View Issue

Multiple adsorption of tributyl phosphate molecule at the dyed-TiO_2/electrolyte interface to suppress the charge recombination in dye-sensitized solar cell

Cite this: *J. Mater. Chem. A*, 2013, **1**, 4885

Molang Cai,[a] Xu Pan,*[b] Weiqing Liu,[a] Jiang Sheng,[a] Xiaqin Fang,[a] Changneng Zhang,[a] Zhipeng Huo,[a] Huajun Tian,[a] Shangfeng Xiao[a] and Songyuan Dai*[a]

Received 25th October 2012
Accepted 31st January 2013

DOI: 10.1039/c3ta00835e

www.rsc.org/MaterialsA

Electron recombination and dye aggregation at the dyed-TiO_2/electrolyte interface are still problems in dye-sensitized solar cell (DSC) research. In this paper, tributyl phosphate (TBpp) as a special additive to modify the dyed-TiO_2/electrolyte interface was introduced to enhance the photovoltaic performance. The adsorption mode of TBpp and the interaction between *cis*-dithiocyanate-*N*,*N*′-bis-(4-carboxylate-4-tetrabutylammonium carboxylate-2,2′-bi-pyridine) ruthenium(II) (N719) and TBpp were investigated. It was found that one TBpp parent molecule split into several smaller fragments and formed four anchoring modes on the TiO_2 surface. It was very interesting that the molecular cleavage of TBpp and adsorption of N719 assisted each other on the sensitized TiO_2 surface. The fragments distributed around N719 result in steric hindrance, consequently hydrogen-bonding among N719 molecules was decreased. The unstable type N719 transformed into stable type N719 accompanied by molecular cleavage of TBpp and the N719 aggregation was reduced. Furthermore, these new fragments were multiply adsorbed on the non-sensitized TiO_2 surface to form an insulating barrier layer. Therefore, the electron recombination at the dyed-TiO_2/electrolyte interface was restrained. Besides the change of surface configuration, the TiO_2 band edge negatively shifted and the rate of electron transport in the TiO_2 films decreased with the addition of TBpp. As a result, an increase in the photoelectric conversion efficiency (η) was obtained of almost 40%.

1 Introduction

Dye-sensitized solar cells (DSCs) have been intensively investigated and developed due to their high efficiency, simple fabrication process and low production cost, since O'Regan and Grätzel first reported them in 1991.[1–7] The dyed-TiO_2/electrolyte interface, made up of sensitized TiO_2 film and electrolyte, is a very complicated interface in DSCs. Two important processes related to the photoelectric conversion efficiency (η), electron injection and electron recombination, are involved at this interface. The upward shift of the LUMO or downward shift of the TiO_2 conduction band should enlarge the energy level mismatch to enhance the electron injection efficiency (η_i) and improve the short-circuit photocurrent (J_{sc}).[8] The downward shift of the TiO_2 conduction band has a negative effect on the open voltage (V_{oc}) due to a narrowing of the gap between the TiO_2 conduction band and the redox electrolyte level. The adsorption of N719 on the TiO_2 surface is accompanied by the deprotonation process of carboxylic groups, which elevates the LUMO of the dye. According to the different thermodynamic stability of various anchoring modes, N719 molecules exhibit singly bond type (unstable type) or two bond (stable type) dyes on the TiO_2 surface.[9] Hydrogen-bonds are formed among N719 molecules with the appearance of an unstable type dye or dye multilayers, which cause dye aggregation and decreases the η_i.[10,11] So it is necessary to restrain the dye aggregation to enhance the η_i of the electron injection process. The injected electrons' transport through the TiO_2 film is accompanied by electron recombination at the dyed-TiO_2/electrolyte interface.[12] The main recombination pathway derives from recapture of the light-induced electrons by the oxidized dye or back reaction with oxidized species in the electrolyte, such as I_3^-. The latter reaction is the main way of recombination and should be restrained due to its harmful effect on the cell performance.[13–15]

TiO_2 surface modification is an effective method to improve the performance of DSCs. Most studies focus on treating TiO_2 surface with $TiCl_4$ [6] and various acids,[16] or coating TiO_2 with inorganic oxide thin layers.[14,17–19] Various kinds of co-adsorbents[20–23] are also added to the dye solution to suppress the

[a]*Key Lab of Novel Thin Film Solar Cells, Institute of Plasma Physics, Chinese Academy of Sciences, P.O. Box 1126, Hefei, Anhui 230031, People's Republic of China. E-mail: sydai@ipp.ac.cn*

[b]*Key Lab of Novel Thin Film Solar Cells, Institute of Plasma Physics, Chinese Academy of Sciences, P.O. Box 1126, Hefei, Anhui 230031, People's Republic of China. E-mail: mars_dark@hotmail.com*

electron recombination. Adding additives into the basic electrolyte provides an easy and convenient way to modify the TiO_2 surface.[24] Some additives, such as 4-*tert*-butylpyridine (TBP),[25–27] *N*-methylbenzimidazole (NMBI) and benzimidazole (BI),[28] adsorb onto the exposed TiO_2 surface, forming an insulating layer that restrains electron recombination and elevates the TiO_2 conduction band. This type of additive improves the V_{oc}, while reducing the J_{sc} simultaneously. The other additive, anhydrous lithium iodide (LiI),[29–31] for example, is found to cause a high η_i and thus enhance the J_{sc}. Unfortunately, this type of additive reduces the V_{oc} by a downward shift of the TiO_2 conduction band. Therefore, it is necessary to develop a type of additive which enables an increase in V_{oc}, while maintaining a high J_{sc} to further enhance the performance of DSCs.

So far, the interaction between additives and dye at the TiO_2 surface is unclear, and the influence of this interaction on the transport and recombination processes in DSCs has not been paid much attention. It is important to understand these relationships to improve the performance of DSCs. In this paper, tributyl phosphate (TBpp) was introduced in the electrolyte to modify the dyed-TiO_2/electrolyte interface. TBpp was demonstrated to reduce the resistance of acetonitrile-based electrolyte.[32] By analyzing the infrared (IR) and UV-vis absorption spectra, we aimed to further investigate the molecular cleavage of TBpp and the interaction between TBpp and N719 at the dyed-TiO_2/electrolyte interface. Meanwhile, a detailed analysis and discussion were made on the influence of the interactions between TBpp and N719 on the transport and recombination processes in DSCs.

2 Experimental

2.1 Sample preparation

TBpp, *N*-methylimidazole, and 1-iodopropane were purchased from Aldrich and were used as received. 1,2-Methyl-3-propylimidazolium iodide (DMPII) was prepared by quaternization of 1-methylimidazole and 1-iodopropane, as reported previously,[33] and its purity was confirmed by ^1H NMR spectroscopy. The standard electrolyte (electrolyte A) for DSCs was 0.08 mol L^{-1} iodine (I_2, 99%, Aldrich), 0.1 mol L^{-1} anhydrous lithium iodide (LiI, 99%, Aldrich), and 1 mol L^{-1} DMPII in acetonitrile (ACN, 99%, Sinopharm chemical reagent). To prepare electrolyte B, 1 mol L^{-1} TBpp was added into the standard electrolyte. Electrolyte A and electrolyte B were used to assemble device A, and device B respectively.

The TiO_2 paste was printed onto transparent conducting glass sheets and sintered in air at 450 °C for 30 min. The thickness of the film was about 14 μm and the active area was 0.25 cm^2. For higher efficiency, the freshly sintered TiO_2 films were immersed into 0.05 mol L^{-1} $TiCl_4$ aqueous solution and stored in a closed vessel at 60 °C for 30 min. After washing with distilled water and drying, the films were sintered again at 450 °C for 30 min. Then these samples were cooled to 120 °C and were immersed in an anhydrous ethanol solution with 5.0×10^{-4} mol L^{-1} N719 for 12 h. The counter electrode was platinized by H_2PtCl_6 spraying solution on transparent conducting glass and fired in air at 410 °C for 20 min. Then, it was placed directly on top of the dye-sensitized TiO_2 films. The gap between the two electrodes was sealed by thermal adhesive (Surlyn, Dupont). The electrolyte was filled through a hole on the counter electrode, and the hole was later sealed with a cover glass and thermal adhesive film.

The samples for ATR-FTIR and UV-vis can be prepared in the following way. The TiO_2 films (5 μm) were respectively immersed in a 1 mol L^{-1} TBpp acetonitrile solution (TBpp/TiO_2) for 12 h and an ethanol solution of 0.5 mmol L^{-1} N719 (N719/TiO_2). These samples were then rinsed with ethanol three times and dried under vacuum state at room temperature. Thereafter, one of the dyed-TiO_2 films was dipped into the 1 mol L^{-1} TBpp acetonitrile solution for 12 h (TBpp/N719/TiO_2). Then the coated film was rinsed with acetonitrile and dried in vacuum state at room temperature.

2.2 Measurements

The photocurrent–voltage (*I–V*) characteristics of the DSC were obtained using a Keithley 2420 digital source meter (Keithley, USA), under a 450 W xenon lamp (Oriel, USA) with a filter (AM 1.5). Intensity modulated photocurrent spectroscopy and intensity modulated photovoltage spectroscopy (IMPS/IMVS) measurements were performed on an IM6ex (Germany, Zahner Company) using light emitting diodes ($\lambda = 610$ nm) driven by Export (Germany, Zahner Company). The LED provided both the dc and ac components of the illumination. A small ac component is 10% or less than that of the dc component and the frequency range was 3 kHz to 0.3 Hz. Electrochemical impedance spectroscopy (EIS) measurements were also recorded with IM6ex, at a perturbation amplitude of 5 mV within the frequency range from 3 MHz to 5 mHz in the dark. The IR spectra for all the samples were measured by using a NICOLET8700 FTIR spectrometer (USA, Thermo Fisher Scientific). Absorption spectra were performed on a Hitachi U-3010 UV-vis spectrophotometer from 400 nm to 800 nm.

3 Results and discussion

3.1 Infrared results for anchoring modes

Fig. 1(a) compares the infrared (IR) spectra of neat TBpp with TBpp/TiO_2 to investigate the anchoring mode of TBpp on the TiO_2 surface. The characteristic absorption bands of TBpp present at 1282 cm^{-1} and near 1027 cm^{-1} are attributed to ν(P═O) and ν(C–O), respectively.[34] The peak at 910 cm^{-1} belongs to the stretching vibration of P–O–C. The bands observed at 1469 cm^{-1} and 1384 cm^{-1} are due to the bending vibration of $\delta(CH_2)$ and $\delta(CH_3)$, respectively.[35] The weak bands at 1118 cm^{-1} and 1151 cm^{-1} are the skeletal vibrations of the C–C bond and the signal of butoxy. The ν(P═O) of TBpp which occurs at 1282 cm^{-1} for TBpp in the neat sample, is shifted to 1202 cm^{-1} upon adsorption on the TiO_2 surface.[36] This large shift of the P═O stretching mode is ascribed to the environmental sensitivity of the phosphoryl group.[37] However, the position of the carbon–oxygen stretching mode of TBpp (1027 cm^{-1}) is not changed, which indicates that some butoxy moieties are not involved in the adsorption of phosphoryl groups. In the

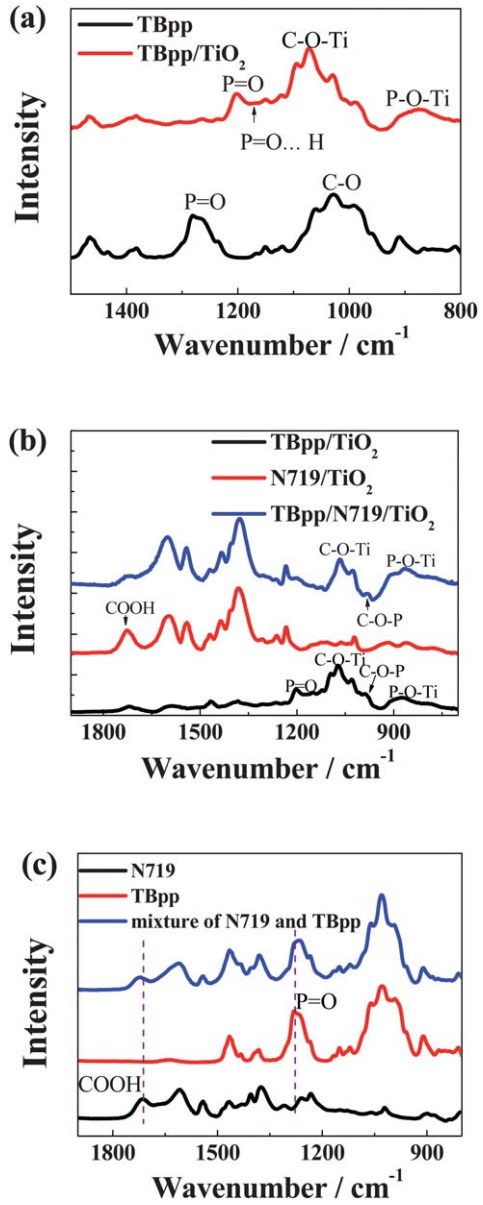

Fig. 1 (a) FTIR spectra of neat TBpp and ATR-FTIR spectra of TBpp/TiO_2, (b) ATR-FTIR spectra of N719/TiO_2, TBpp/N719/TiO_2, (c) FTIR spectra of N719 power, neat TBpp and N719 powder with TBpp. All of the ATR-FTIR spectra of samples on the TiO_2 film were obtained by subtracting off the blank TiO_2 film sample.

TBpp/TiO_2 sample, a wide band is found near 1200 cm^{-1} due to the P═O···H bond and a new wide band near 879 cm^{-1} is attributed to ν(P–O–Ti). In addition, the intensity of ν(P═O) decreases dramatically in the TBpp/TiO_2 sample. This effect indicates that the P═O moiety no longer exists with a double bond, but has intermediate character between a single and a double bond. It is expected that all these vibrations will be influenced by delocalization of the electrons. The new vibrational mode at 1071 cm^{-1} appears due to ν(C–O) of C–O–Ti bonds[38,39] as a loss of the intensity of the P–O–C moiety occurs at 1027 cm^{-1}. This may be interpreted as $CH_3CH_2CH_2O$– moieties of the phosphorus atoms being removed and adsorbing on the TiO_2 surface. The formation of butoxy groups occurs in parallel with the obvious decrease of the P═O mode in the adsorption process. According to the experimental data analysed above and in previous reports,[35,36] it can be deduced that the adsorption of TBpp on the TiO_2 surface leads to one parent molecule splitting into several fragment ions. Three $CH_3CH_2CH_2O$– ligands of the phosphorus atom split from the parent molecule equally, and consequently four anchoring modes on the TiO_2 surface will be obtained, as shown in Scheme 1. Similar to reports for titanium oxide–alkoxide–phosphonate complexes, the main bonding mode to the surface should involve quadridentate units.[40] In our research, the presence of stretching of the carbon–oxygen stretching mode of TBpp at 1027 cm^{-1} suggests the presence of residual P–$OCH_2CH_2CH_3$ groups in the other three types of adsorption modes.

The N719 complex contains two carboxylic groups and two carboxylate groups. The carboxylic groups are *trans* to each other, and the carboxylate groups are *trans* to the NCS ligands. The dye molecules attached *via* two groups coming from two different bipyridines, are thermodynamically most favorable.[11,41] So the anchoring mode *via* a single group (two groups) is called the unstable type mode (stable type mode). The unstable type N719 anchors on the TiO_2 surface through one carboxylic group, leaving the other carboxylic group free. When the carboxylic group of N719 is present, hydrogen-bonds might be formed between two carboxylic groups from two different N719 molecules. Dye aggregation caused by hydrogen-bonds decreases the J_{sc} of DSCs.[42] The stable type N719 in the thermodynamically most favorable state anchors onto the TiO_2 surface with two carboxylic groups which left no free carboxylic groups. The reduction in free carboxylic acid groups leads to a decrease of hydrogen-bonding aggregation among N719, and hence the decrease in electron recombination and the improvement of the J_{sc}.[43] The ATR-FITR spectra of TBpp/TiO_2, N719/TiO_2 and TBpp/N719/TiO_2 are compared in Fig. 1(b). The N719/TiO_2 shows strong bands at 1609 cm^{-1} and 1375 cm^{-1} due to ν_{as}(–COO^-) and ν_s(–COO^-), respectively, of carboxylate groups anchored to the surface of the TiO_2.[9] The bands at 1715 cm^{-1} and near 1260 cm^{-1} are attributed to ν(C═O) and

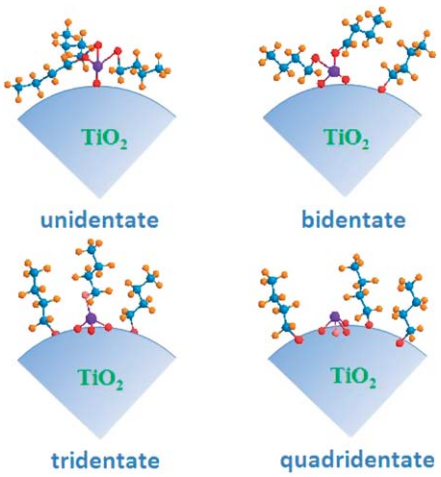

Scheme 1 Schematic representations of the possible bonding modes of TBpp molecules on the TiO_2 surface.

ν(C–O) of the free carboxylic acid of N719.[44] The ν(C=C) modes of pyridine groups are observed at 1542 cm^{-1} and 1405 cm^{-1}.[45] The intensity at 1715 cm^{-1} relative to that at 1375 cm^{-1} indicates the relative amounts of unstable and stable type dye molecules on the TiO_2 surface.[11] The stable type and unstable type modes both exist when N719 absorbs on the TiO_2 surface alone. After the sensitized films was stained with TBpp, ν(C=O) located at 1715 cm^{-1} decreases dramatically with the increase of $\nu_{as}(-COO^-)$, indicating that the unstable type mode transforms into the stable type mode. As a result, the addition of TBpp causes the decrease of hydrogen-bonding aggregation in N719.[42,46]

In addition, comparing the TBpp/TiO_2 with the TBpp/N719/TiO_2 sample, the ν(P=O) located at 1202 cm^{-1} hardly disappears, which indicates the coordination of all of the phosphoryl oxygens to surface Lewis acid sites.[35] However, there are still residual P=O···H bonds near 1020 cm^{-1} which may be caused by intermolecular hydrogen-bonds. The FTIR spectra of N719 powder, neat TBpp and a mixture of N719 with TBpp (molar ratio of N719 to TBpp is 1 : 1) are obtained, as shown in Fig. 1(c) to define the hydrogen-bonds between TBpp and N719. The band of ν(C=O) in N719 slightly red shifts from 1715 cm^{-1} to 1728 cm^{-1}, and the band at 1282 cm^{-1} due to ν(P=O) in TBpp slightly blue shifts. This is convincing evidence that the carboxylic group of N719 acts as a proton donor and the phosphonyl group of TBpp acts as a proton acceptor, forming a hydrogen-bond.

Scheme 2 shows the unstable type N719 transforming into stable type N719, accompanied by the possible anchoring process of TBpp. One TBpp parent molecule splits into several smaller fragments and then adsorbs onto the TiO_2 surface, acting as an insulation layer. These new fragments are inserted among the N719 molecules, forming steric hindrance, which inhibits the intermolecular hydrogen-bonds of dye molecules and the unstable type N719 transforming into stable type.

3.2 Photovoltaic performance and the kinetics of electron transfer

Fig. 2 presents the *I–V* curves under full sun illumination and the dark current for device A and device B. The photovoltaic performances, V_{oc}, fill factor (FF), J_{sc} and η for device A and device B, are listed in Table 1. It is notable that the addition of TBpp enhances the V_{oc} by 160 mV and increases the J_{sc} by 1.43 mA cm^{-2}, resulting in a 40% improvement of the η (9.50%). The dark current of device B decreases, which indicated that a decrease of dark current is achieved by the addition of TBpp.

Fig. 3 shows the typical Nyquist plot of two devices measured in the dark under a forward bias of −0.62 V. Three semi-circles are observed with gradually increasing frequency in a typical electrochemical impedance spectroscopy (EIS) Nyquist plot of a DSC. In the range of high frequency, the first semi-circle corresponds to the charge transfer process at the counter electrode/electrolyte interface. The second semi-circle in the middle-frequency range corresponds to the recombination process at the dyed-TiO_2/electrolyte interface. The third semi-circle occurring in the low frequency range is attributed to the ion diffusion within the electrolyte. The equivalent circuit used for fitting the impedance spectra of the DSC is shown in the inset of Fig. 3. In the equivalent circuit, R_s, R_{CE}, R_{ct} and R_w represent series resistance, charge transfer resistance at the counter electrode/electrolyte interface, electron recombination resistance at the dyed-TiO_2/electrolyte interface and Nernst diffusion impedance, respectively. C_μ and C_p are attributed to the chemical capacitance at the dyed-TiO_2/electrolyte interface and the counter electrode/electrolyte interface, respectively.

The V_{oc} is determined by the difference between the electron quasi-Fermi level in the TiO_2 film and the redox potential of the electrolyte. Electron recombination plays a significant role in reducing the electron density in the TiO_2 film. The increase of R_{ct} indicates the decrease of electron recombination as a means of increasing electron density. More electron accumulation in the TiO_2 film can cause the electron quasi-Fermi level to shift upward, leading to a higher V_{oc}.

Fig. 4 shows the fitting results for device A and device B using the equivalent circuit in the inset of Fig. 3. The EIS measurements are carried out in the dark at different bias voltages between −0.50 V and −0.72 V. As shown in Fig. 4(a), R_{ct} of both devices exhibits an exponential decrease when going towards negative biases. The values of R_{ct} can be evaluated using eqn (1): [47,48]

$$R_{ct} = R_0 \exp\left(-e\frac{\beta V}{k_B T}\right) \quad (1)$$

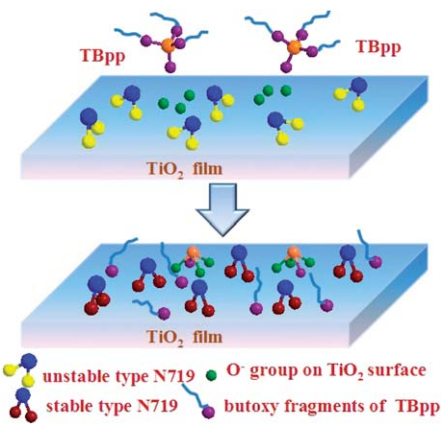

Scheme 2 The process of interaction between the molecular cleavage of TBpp and the adsorption mode transformation of N719.

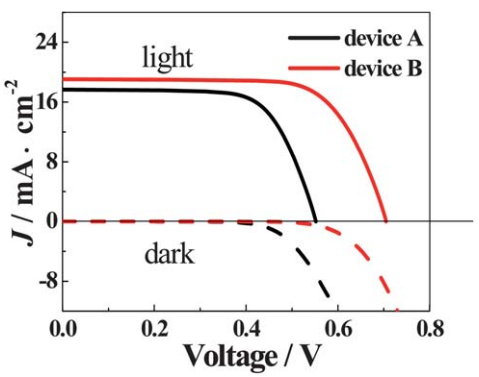

Fig. 2 Photocurrent–voltage characteristics of device A and device B under AM 1.5 sunlight (100 mW cm^{-2}) illumination (solid line) and in the dark (dashed line).

Table 1 Photovoltaic parameters for device A and device B[a]

Device	V_{oc} (V)	J_{sc} (mA cm^{-2})	FF	η (%)
A	0.55	17.68	0.69	6.74
B	0.71	19.11	0.70	9.50

[a] The spectral distribution of the lamp simulated AM 1.5 and sunlight corresponded to an intensity of 100 mW cm^{-2}. The cell performances are obtained when the interfaces of devices tend to be in a relatively stable state.

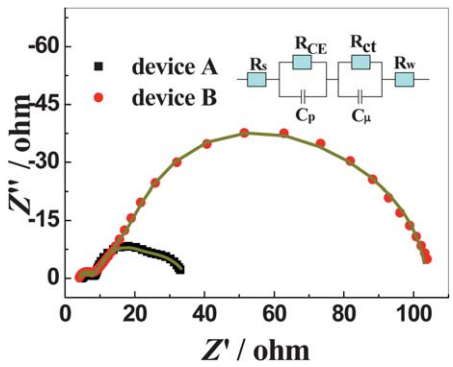

Fig. 3 Impedance spectra of device A and device B measured under dark conditions with an external potential of −0.62 V. The inset shows the equivalent circuit.

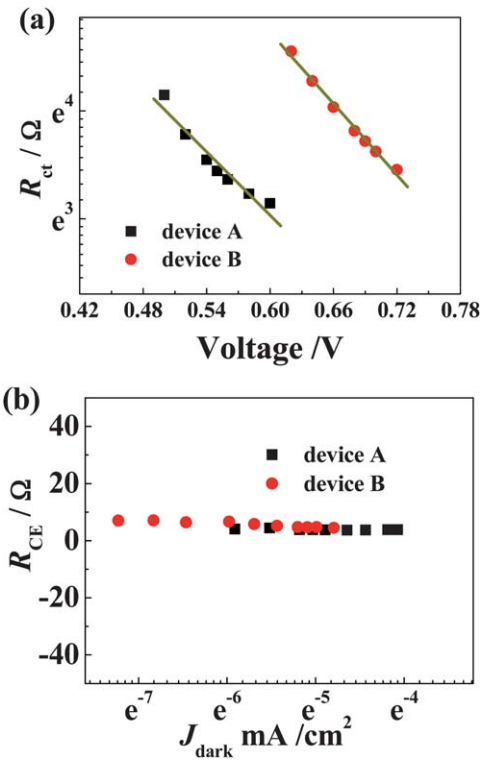

Fig. 4 Typical equivalent circuit elements obtained from EIS at different bias near their open-circuit potentials in the dark for device A and device B; (a) recombination resistance (R_{ct}) at the dyed-TiO_2/electrolyte interface; (b) charge transfer resistance (R_{CE}) at the counter electrode/electrolyte interfaces (R_{CE} *versus* dark current density).

where R_0 is a constant, e is the electron charge, V is the bias voltage, k_B is the Boltzmann constant, T is the absolute temperature and β is the transfer coefficient, which corresponds to the reciprocal value of the diode quality factor. At any given bias voltage, R_{ct} values of device B are higher compared to device A, indicating that the addition of TBpp resulted in a dramatic increase of the R_{ct}. As mentioned in the analysis for IR, the adsorption of fragments from TBpp molecular cleavage forms an insulation layer to block the route between I_3^- and light-induced electrons. In addition, adsorption of TBpp also reduces the aggregation of dye.[49] Thus, the suppression of electron recombination is caused by the combined effects of increased R_{ct} and decreased aggregation of dye.

Fig. 4(b) presents the R_{CE} at the counter electrode/electrolyte interface. At a given dark current, there are very small differences of R_{CE} between device B and device A. This result rules out the effect from the overpotential occurring at the counter electrode with TBpp.

Electron recombination occurs mainly *via* surface states or the TiO_2 conduction band. If electrons directly have recombination reactions *via* the TiO_2 conduction band, β should equal to 1.[50] The values of β are 0.25 and 0.28 for device A and device B, which is obtained from the slope of the straight line, as illustrated in Fig. 4(a). Both values of β are less than 1, indicating that electrons mainly have recombination reactions *via* the surface states rather than *via* the TiO_2 conduction band. This result suggests that the recombination pathway at the dyed-TiO_2/electrolyte interface is not affected by TBpp. Some studies reported that a higher value of β would correspond to a higher value of the FF.[51] Device B gives a higher β when compared to device A, indicating that addition of TBpp could elevate the FF of device A. As shown in Table 1, *I–V* measurement results show that the FF increases slightly with the addition of TBpp, as expected.

To further investigate the electron recombination, the kinetics of electron transfer at the dyed-TiO_2/electrolyte interface are generally discussed from the results of intensity modulated photocurrent spectroscopy and intensity modulated photovoltage spectroscopy (IMVS/IMPS) measurements (Fig. 5). The electron lifetime (τ_n) can be calculated directly from the IMVS response.[52] The greater τ_n gets, the slower the recombination between electrons and I_3^- will be. Fig. 5(a) describes τ_n for both devices with an open circuit over a range of the J_{sc}. The values of τ_n show an exponential decrease with increasing J_{sc}. The τ_n of device B is higher compared to device A at any given J_{sc}, certifying that the rate of electron recombination is slowed down by the passivation of TBpp at the dyed-TiO_2/electrolyte interface.

The improvement of the V_{oc} depends not only on the suppression of recombination, but also on the TiO_2 conduction band shift. The charge buildup on the surface of TiO_2 particles causes the variation of potential across the Helmholtz layer, resulting in the TiO_2 conduction band edge movement.[53] For example, positive (negative) charge buildup gives rise to the band edges shifting downward (upward), toward positive

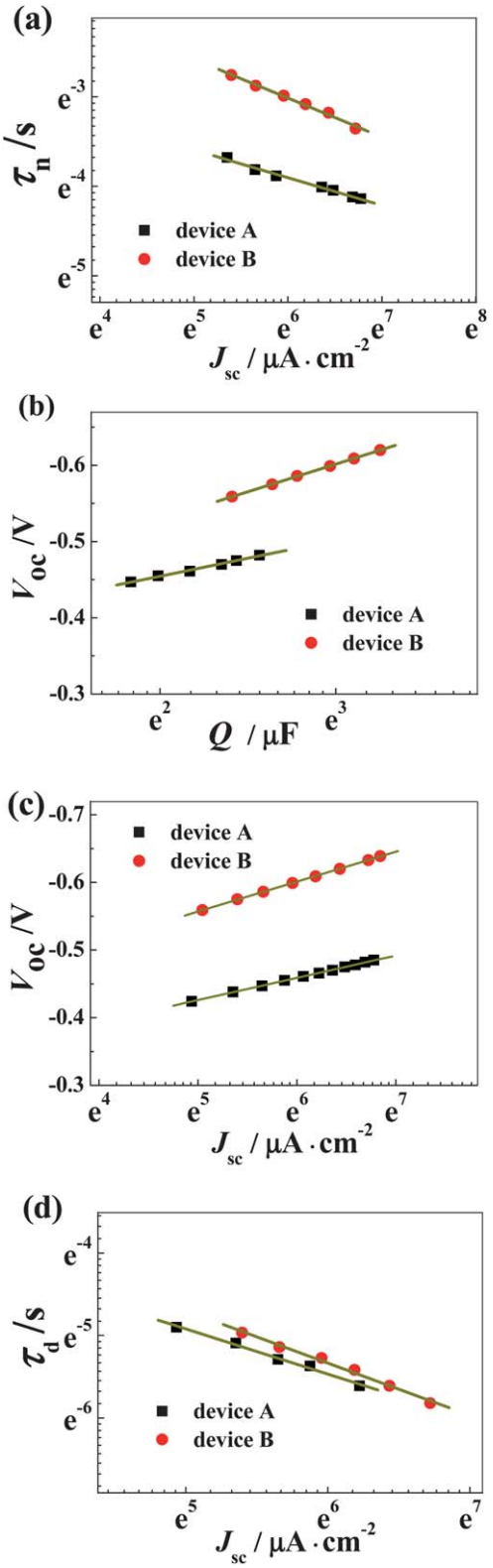

Fig. 5 Relationship between (a) τ_n and J_{sc}, (b) V_{oc} and Q, (c) V_{oc} and J_{sc}, (d) τ_d and J_{sc} with and without TBpp.

(negative) electrochemical potentials, which leads to the decrease (increase) of the V_{oc}. As we know, there is a major feature in the nanoporous TiO_2 film that a huge number of excess electrons can be stored in this network. The difference between the TiO_2 conduction band edge and the quasi-Fermi level depends on the photoinduced charge (Q).[46] For a given Q, the increase in V_{oc} is attributed to an upward shift of the TiO_2 conduction band. On the contrary, the decrease in V_{oc} is attributed to a downward shift of the TiO_2 conduction band. In the open circuit, Q is obtained from $Q = J_{sc} \times \tau_n$.[54] Fig. 5(b) depicts the dependence of V_{oc} on ln(Q) in TiO_2 at open circuit according to eqn (2): [53]

$$V_{oc} = V_0 + m_0 \ln Q \quad (2)$$

where V_0 is the vertical intercept and m_0 is the slope, that is, $m_0 = dV_{oc}/d\ln Q$. As mentioned in the analysis of ATR-FTIR, the fragments of TBpp molecules anchor onto the TiO_2 surface by forming P–O–Ti bonds and C–O–Ti bonds. The oxygen atoms act as electron donors which provide negative charge to the dyed-TiO_2/electrolyte interface. Compared to device A, a negative band shift of device B causes an increase in the V_{oc} by ~80 mV at constant Q. Fig. 5(c) shows that the relationship between current and voltage under monochromatic light. The V_{oc} obviously increases after the addition of TBpp, caused by elevating the TiO_2 conduction band and decreasing electron recombination. This result is consistent with the I–V tests under full sun illumination.

Due to the small size of the TiO_2 particles and the effect of electrolyte shielding, the driving force for electron transport in the TiO_2 film is the electron concentration gradient in the film, but not electric field action.[55] The electron transit time (τ_d) is associated with electron transport in porous TiO_2 film, which can be obtained directly from IMPS.[52] The relationship between τ_d and J_{sc} can be described as following the exponential distribution in eqn (3): [56]

$$\tau_d \propto J_{sc}^{\alpha-1} \quad (3)$$

where the parameter α is related to the steepness of the trap-state distribution. As predicted in Fig. 5(d), τ_d is a function of the J_{sc} in double logarithmic form and τ_d decrease with the increase of the J_{sc} in both devices. At constant J_{sc}, the τ_d of device B slightly increases compared with device A. The slope of the ln(τ_d) *versus* ln(J_{sc}) plot, which reflects the trap-state distribution of the TiO_2 surface is described by α in eqn (3).[57] The values of α are 0.45 and 0.37 for device A and device B, respectively. This result predicted that the addition of TBpp slightly changes the distribution of surface states. The decrease of α is ascribed to the widening of the exponential conduction band, and corresponds to a steeper trap state distribution, which may slow down the electron transport process.[58]

In addition, another possible reason for slow electron transport can be considered. In the presence of TBpp, the TiO_2 conduction band's negative shift impairs electron injection. The condition of the grain boundaries between TiO_2 particles can influence electron transport.[59] Some of the TBpp molecules covered the surface of joints between TiO_2 particles, hindering the electron transport and thus increasing τ_d.

The competition between electron recombination and electron transportation of injected electrons are measured by the effective electron diffusion length:[60]

$$L = d\sqrt{\tau_n/2.35\tau_d} \quad (4)$$

The longer L reflects the higher electron collection efficiency (η_c), which has a positive effect on the J_{sc}.[61] Fig. 6 compares the L of device A with device B to define the difference in η_c with and without TBpp. The value of L is higher with the addition of TBpp, which is independent of the Q in the TiO_2 film. This indicates that the restraint of electron recombination by TBpp modification is the main effect in the competition. As a result, the lower loss of electrons in the photoelectric conversion process leads to the enhancement of J_{sc}.

Conclusions

Our study introduced the multiple adsorption of TBpp onto the TiO_2 surface to modify the dyed-TiO_2/electrolyte interface, resulting in the remarkable enhancement of cell performance. The TBpp acting as parent molecule split into several smaller fragments. The new fragments were widely distributed on the non-sensitized TiO_2 surface to form an insulating barrier to restrict electron recombination. The decrease of electron recombination has positive effects on both J_{sc} and V_{oc}. It was very interesting that the molecular cleavage of TBpp and adsorption of N719 assisted each other. The TBpp cleaved into more fragments and these new fragments inserted among N719 molecules, which inhibit dye aggregation to enhance the J_{sc}. Moreover, the electronegative oxygen atoms acted as electron donors to elevate the TiO_2 conduction band. So the device with TBpp exhibited an increase of V_{oc} by 160 mV when TBpp co-absorbed with N719. As a result, both the V_{oc} and J_{sc} were improved by the addition of TBpp in the electrolyte to obtain a higher η of 9.50%. These quantitative results drew attention to a new perspective to enhance the photovoltaic efficiency by introducing a novel molecular adsorption mode.

Acknowledgements

This work is financially supported by the National Basic Research Program of China under Grant No. 2011CBA00700, the National High Technology Research and Development Program of China under Grant No. 2010AA050510, the National Natural Science Foundation of China under Grant No. 21273242, the National Natural Science Foundation of China under Grant No. 21173227, the National Natural Science Foundation of China under Grant No. 21103197 and National Natural Science Foundation of China under Grant No. 21003130.

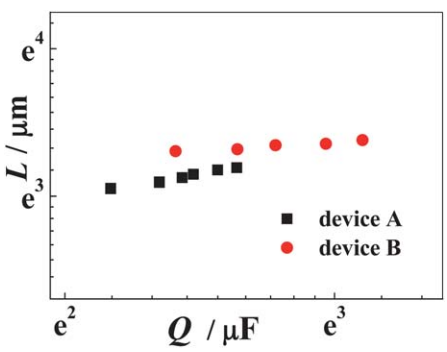

Fig. 6 Effective electron diffusion length (L) as a function of Q derived from IMVS and IMPS measurements for device A and device B.

Notes and references

1 B. Oregan and M. Gratzel, *Nature*, 1991, **353**, 737–740.
2 J. H. Yum, E. Baranoff, F. Kessler, T. Moehl, S. Ahmad, T. Bessho, A. Marchioro, E. Ghadiri, J. E. Moser, C. Y. Yi, M. K. Nazeeruddin and M. Gratzel, *Nat. Commun.*, 2012, **3**, 631.
3 Y. J. Kim, J. H. Kim, M. S. Kang, M. J. Lee, J. Won, J. C. Lee and Y. S. Kang, *Adv. Mater.*, 2004, **16**, 1753–1757.
4 M. X. Wu, X. Lin, Y. D. Wang, L. Wang, W. Guo, D. D. Qu, X. J. Peng, A. Hagfeldt, M. Gratzel and T. L. Ma, *J. Am. Chem. Soc.*, 2012, **134**, 3419–3428.
5 F. Gao, Y. Wang, D. Shi, J. Zhang, M. K. Wang, X. Y. Jing, R. Humphry-Baker, P. Wang, S. M. Zakeeruddin and M. Gratzel, *J. Am. Chem. Soc.*, 2008, **130**, 10720–10728.
6 T. C. Li, A. M. Spokoyny, C. She, O. K. Farha, C. A. Mirkin, T. J. Marks and J. T. Hupp, *J. Am. Chem. Soc.*, 2010, **132**, 4580–4582.
7 M. Marszalek, S. Nagane, A. Ichake, R. Humphry-Baker, V. Paul, S. M. Zakeeruddin and M. Gratzel, *J. Mater. Chem.*, 2012, **22**, 889–894.
8 N. Kopidakis, N. R. Neale and A. J. Frank, *J. Phys. Chem. B*, 2006, **110**, 12485–12489.
9 M. K. Nazeeruddin, R. Humphry-Baker, P. Liska and M. Gratzel, *J. Phys. Chem. B*, 2003, **107**, 8981–8987.
10 M. Liang, M. Lu, Q. L. Wang, W. Y. Chen, H. Y. Han, Z. Sun and S. Xue, *J. Power Sources*, 2011, **196**, 1657–1664.
11 V. Shklover, Y. E. Ovchinnikov, L. S. Braginsky, S. M. Zakeeruddin and M. Gratzel, *Chem. Mater.*, 1998, **10**, 2533–2541.
12 A. B. Walker, L. M. Peter, M. J. Cass, P. J. Cameron and D. Martinez, *J. Mater. Chem.*, 2005, **15**, 2253–2256.
13 M. Gratzel, *Nature*, 2001, **409**, 575–576.
14 E. Palomares, J. N. Clifford, S. A. Haque, T. Lutz and J. R. Durrant, *J. Am. Chem. Soc.*, 2003, **125**, 475–482.
15 A. J. Frank, N. Kopidakis and J. van de Lagemaat, *Coord. Chem. Rev.*, 2004, **248**, 1165–1179.
16 S. C. Hao, J. H. Wu, L. Q. Fan, Y. F. Huang, H. M. Lin and Y. L. Wei, *Sol. Energy*, 2004, **76**, 745–750.
17 S. H. A. Lee, Y. X. Zhao, E. A. Hernandez-Pagan, L. Blasdel, W. J. Youngblood and T. E. Mallouk, *Faraday Discuss.*, 2012, **155**, 165–176.
18 D. B. Menzies, Q. Dai, Y. B. Cheng, G. P. Simon and L. Spiccia, *C. R. Chim.*, 2006, **9**, 713–716.
19 H. S. Jung, J. K. Lee, M. Nastasi, S. W. Lee, J. Y. Kim, J. S. Park, K. S. Hong and H. Shin, *Langmuir*, 2005, **21**, 10332–10335.

20 A. Morandeira, I. Lopez-Duarte, B. O'Regan, M. Victoria Martinez-Diaz, A. Forneli, E. Palomares, T. Torres and J. R. Durrant, *J. Mater. Chem.*, 2009, **19**, 5016–5026.
21 K. Hara, Y. Dan-Oh, C. Kasada, Y. Ohga, A. Shinpo, S. Suga, K. Sayama and H. Arakawa, *Langmuir*, 2004, **20**, 4205–4210.
22 P. Wang, S. M. Zakeeruddin, R. Humphry-Baker and M. Gratzel, *Chem. Mater.*, 2004, **16**, 2694–2696.
23 P. Wang, S. M. Zakeeruddin, R. Humphry-Baker, J. E. Moser and M. Gratzel, *Adv. Mater.*, 2003, **15**, 2101–2104.
24 S. Raja, C. Satheeshkumar, P. Rajakumar, S. Ganesan and P. Maruthamuthu, *J. Mater. Chem.*, 2011, **21**, 7700–7704.
25 S. Y. Huang, G. Schlichthorl, A. J. Nozik, M. Gratzel and A. J. Frank, *J. Phys. Chem. B*, 1997, **101**, 2576–2582.
26 G. Boschloo, L. Haggman and A. Hagfeldt, *J. Phys. Chem. B*, 2006, **110**, 13144–13150.
27 H. Greijer, J. Lindgren and A. Hagfeldt, *J. Phys. Chem. B*, 2001, **105**, 6314–6320.
28 H. Kusama and H. Arakawa, *J. Photochem. Photobiol., A*, 2004, **162**, 441–448.
29 S. Pelet, J. E. Moser and M. Gratzel, *J. Phys. Chem. B*, 2000, **104**, 1791–1795.
30 S. H. A. Lee, A. M. S. Jackson, A. Hess, S. T. Fei, S. M. Pursel, J. Basham, C. A. Grimes, M. W. Horn, H. R. Allcock and T. E. Mallouk, *J. Phys. Chem. C*, 2010, **114**, 15234–15242.
31 D. F. Watson and G. J. Meyer, *Coord. Chem. Rev.*, 2004, **248**, 1391–1406.
32 S. J. Xu, Y. F. Luo, S. G. Li, W. Zhong and M. D. Huang, *J. Inorg. Mater.*, 2012, **27**, 83–88.
33 C. W. Shi, S. Y. Dai, K. J. Wang, L. Guo, X. Pan, F. T. Kong and L. H. Hu, *Acta Phys.-Chim. Sin.*, 2005, **21**, 534–538.
34 E. Y. Bae, W. Y. Choi, J. W. Park, H. S. Shin, S. B. Kim and J. S. Lee, *J. Phys. Chem. B*, 2004, **108**, 14093–14101.
35 C. N. Rusu and J. T. Yates, *J. Phys. Chem. B*, 2000, **104**, 12292–12298.
36 G. Guerrero, P. H. Mutin and A. Vioux, *Chem. Mater.*, 2001, **13**, 4367–4373.
37 R. M. Crooks, H. C. Yang, L. J. McEllistrem, R. C. Thomas and A. J. Ricco, *Faraday Discuss.*, 1997, **107**, 285–305.
38 A. Glisenti, *J. Mol. Catal. A: Chem.*, 2000, **153**, 169–190.
39 F. J. Ma, S. X. Liu, C. Y. Sun, D. D. Liang, G. J. Ren, F. Wei, Y. G. Chen and Z. M. Su, *J. Am. Chem. Soc.*, 2011, **133**, 4178–4181.
40 G. Guerrero, M. Mehring, P. H. Mutin, F. Dahan and A. Vioux, *J. Chem. Soc., Dalton Trans.*, 1999, 1537–1538.
41 K. Kilsa, E. I. Mayo, B. S. Brunschwig, H. B. Gray, N. S. Lewis and J. R. Winkler, *J. Phys. Chem. B*, 2004, **108**, 15640–15651.
42 R. Gao, L. Wang, B. Ma, C. Zhan and Y. Qiu, *Langmuir*, 2010, **26**, 2460–2465.
43 Z.-S. Wang and H. Sugihara, *Langmuir*, 2006, **22**, 9718–9722.
44 Y. Park, Y. M. Jung, S. Sarker, J. J. Lee, Y. Lee, K. Lee, J. J. Oh and S. W. Joo, *Sol. Energy Mater. Sol. Cells*, 2010, **94**, 857–864.
45 K. E. Lee, M. A. Gomez, S. Elouatik and G. P. Demopoulos, *Langmuir*, 2010, **26**, 9575–9583.
46 J. Lim, Y. S. Kwon and T. Park, *Chem. Commun.*, 2011, **47**, 4147–4149.
47 L. M. Peter, *Phys. Chem. Chem. Phys.*, 2007, **9**, 2630–2642.
48 F. Fabregat-Santiago, J. Bisquert, G. Garcia-Belmonte, G. Boschloo and A. Hagfeldt, *Sol. Energy Mater. Sol. Cells*, 2005, **87**, 117–131.
49 L. D. Wang, R. Gao, Y. Geng, B. B. Ma, Y. F. Zhu, H. P. Dong and Y. Qiu, *J. Phys. Chem. C*, 2011, **115**, 17986–17992.
50 Q. Wang, Z. Zhang, S. M. Zakeeruddin and M. Gratzel, *J. Phys. Chem. C*, 2008, **112**, 7084–7092.
51 Q. Wang, S. Ito, M. Gratzel, F. Fabregat-Santiago, I. Mora-Sero, J. Bisquert, T. Bessho and H. Imai, *J. Phys. Chem. B*, 2006, **110**, 25210–25221.
52 L. M. Peter and K. G. U. Wijayantha, *Electrochim. Acta*, 2000, **45**, 4543–4551.
53 G. Schlichthorl, S. Y. Huang, J. Sprague and A. J. Frank, *J. Phys. Chem. B*, 1997, **101**, 8141–8155.
54 N. G. Park, G. Schlichthorl, J. van de Lagemaat, H. M. Cheong, A. Mascarenhas and A. J. Frank, *J. Phys. Chem. B*, 1999, **103**, 3308–3314.
55 L. Dloczik, O. Ileperuma, I. Lauermann, L. M. Peter, E. A. Ponomarev, G. Redmond, N. J. Shaw and I. Uhlendorf, *J. Phys. Chem. B*, 1997, **101**, 10281–10289.
56 J. van de Lagemaat and A. J. Frank, *J. Phys. Chem. B*, 2001, **105**, 11194–11205.
57 J. van de Lagemaat and A. J. Frank, *J. Phys. Chem. B*, 2000, **104**, 4292–4294.
58 Z. P. Zhang, S. M. Zakeeruddin, B. C. O'Regan, R. Humphry-Baker and M. Gratzel, *J. Phys. Chem. B*, 2005, **109**, 21818–21824.
59 H. Alarcon, G. Boschloo, P. Mendoza, J. L. Solis and A. Hagfeldt, *J. Phys. Chem. B*, 2005, **109**, 18483–18490.
60 S. Sodergren, A. Hagfeldt, J. Olsson and S. E. Lindquist, *J. Phys. Chem.*, 1994, **98**, 5552–5556.
61 J. Bisquert and V. S. Vikhrenko, *J. Phys. Chem. B*, 2004, **108**, 2313–2322.

